J Intell Robot Syst (2015) 80:325–340
DOI 10.1007/s10846-015-0177-3

Mechatronic System and Experiments of a Spherical Underwater Robot: SUR-II

Chunfeng Yue · Shuxiang Guo · Maoxun Li · Yaxin Li · Hideyuki Hirata · Hidenori Ishihara

Received: 22 January 2014 / Accepted: 2 January 2015 / Published online: 15 January 2015

Abstract This paper describes the structural design of the SUR-II spherical underwater robot. A spherical shape was adopted due to its outstanding shock resistance and flexibility. We designed and developed vectored water-jet thrusters to implement 4-degrees-of-freedom (4-DOF) underwater motion while saving energy. Because each thruster provided 2-DOF motion, three were sufficient for 4-DOF motion. Therefore, the propulsion system was composed of three vectored water-jet thrusters mounted on an equilateral triangular support. A master–slave structure was employed for the electrical design to realize data collection and motion control. The master side was used for the sensor data collection and control algorithm, and the slave side was used to control the propulsion system. After examining the performance of a first-generation electrical system, we chose a more powerful master processor to allow for a more complicated control algorithm. A microelectromechanical system (MEMS) inertial measurement unit replaced the original gyroscope to collect the attitude angle for the three axes. A Kalman filter was used to calibrate the data output and reduce the noise of the MEMS sensor. A series of underwater motion experiments were carried out to test the performance of the spherical underwater robot; these included surge motion, yaw motion, depth control, and multiple-depth control tests. A proportional–derivative (PD) controller was used to control the direction of the vectored water-jet thrusters for underwater motion. The experimental results demonstrated that the spherical underwater robot could realize underwater motion by controlling the direction of the thrusters. However, the robot was not very stable because the change in the propulsive force was nonlinear.

Keywords Spherical underwater robot · Mechnanical structure · Electrical system · Underwater experiment · Vectored water-jet thruster

C. Yue (✉) · M. Li · Y. Li
Graduate School of Engineering, Kagawa University, Takamatsu, Kagawa, Japan
e-mail: chunfengyue@gmail.com; s12d502@stmail.eng.kagawa-u.ac.jp

S. Guo · H. Hirata · H. Ishihara
Faculty of Engineering, Kagawa University, Takamatsu, Kagawa, Japan

S. Guo
School of Life Science and Technology, Beijing Institute of Technology, Beijing, China
e-mail: guo@eng.kagawa-u.ac.jp

1 Introduction

Robots are now widely used for underwater tasks considered by humans to be dangerous, dull, or dirty, primarily because of their long endurance [1], stable high speeds [2], and large load capabilities. The applications of autonomous underwater vehicles (AUVs)

include fields such as ocean research, scientific investigation, ocean development, and underwater projects and may involve pollution detection, submarine sampling and data collection, video mapping, exploration of unstructured underwater environments, and object recovery from dangerous places, as well as other tasks [3–5]. Different tasks require different shapes and sizes of AUVs. For example, a streamlined shape reduces water resistance and is preferable if the vehicle must move at high speeds. Delphin2, Autosub6000 and Canadian Self Contained Off-the-shelf Underwater Testbed (C-Scout) are very typical and famous streamlined AUVs [5–7] and these AUVs are quite suitable for a large area survey. Of course, long cruising ability is also a very important characteristic. The Petrel-II underwater glider can go 1,500 meters underwater; maximum voyage is 1,000 kilometers and it can work 30 days continuously [1, 8]. But if underwater detection or operation tasks are the primary roles of an underwater robot, a non-streamlined shape is often used [4, 9]. Researchers in Spain have developed a Reconfigurable Autonomous Underwater Vehicle for Intervention. This AUV has managed to recover an object similar to an aircraft black box without the direction of any operator [9]. Deep-sea research requires high water-pressure resistance, whereas monitoring and observation tasks require small, flexible, and stable robots [2].

1.1 Related Studies

Roger Stokey et al. developed Remote Environmental Measuring UnitS (REMUS) which is driven only by one propeller and two pairs aft fins. The aft fin is used to realize yaw and pitch motion [10, 11], and the turning radius is about 2 m. In University of Southampton, L. V. Steenson et al. developed a over actuated AUV: Delphin2 not only fins and propeller, but also two tunnel thruster units install onto the front and rear of a pressure vessel to enhance the maneuverability. The Delphin2 can realize 6 DOF motion, turning circle within 2 m (length of the Delphin2) at 0m/s. In Ocean Engineering Research Centre (OERC)-Memorial University of Newfoundland (MUN), Timothy L. Curtis et al. developed a more convenient AUV: C-Scout, this robot adoped modular design, it can be assambed according to custom requirement, baseline configuration (BC) and fully-actuated configuration (FAC) [7]. The actuated method of baseline configuration is almost same as REMUS and the fully-actuated configuration is same as Deiphin2.

Besides streamline shape AUV, other special shapes are also adopted to implement underwater robot. Especially, spherical robots have good water-pressure resistance and can realize rotational motion with a zero turn radius. Many types of spherical underwater robots have been developed. ODIN-III [12, 13] was a typical prototype robot developed at the University of Hawaii. It had a metal shell, a diameter of 630 mm, six screw propellers installed outside the body, and a weight of 150 kg. This spherical underwater robot was used to monitor the environment and perform underwater operations. Researchers at the University of Manchester and Oxford University [14–17] co-developed a micro-spherical underwater robot. This robot employed six propellers located around the equator of its spherical hull for its propulsion system. The diameter was only 150 mm, and a gyroscope was used to measure the angle in the yaw direction. This micro-robot was developed to monitor nuclear storage ponds and wastewater treatment facilities to prevent leakage. Both of these robots used propellers on the outside of their bodies as propulsion systems. The disadvantages of propellers are their high underwater noise and cavitation.

Due to the high-efficiency, low noise and tight structure, tunnel thruster has been used into AUVs frequently, and some researchers has been involved in this research topic. L. V. Steenson et al. [18] also tested the performance of tunnel thrusters on the Dophine2. They analyzed the reason of thrust reduction when the tunnel thruster working on a free surface and obtained the result when the tunnel thruster in different speed. Alistair Palmer et al. [19] carried out an experimental test and established a turnnel thruster model to show how the thrust forces and moments effect on the vehicle. Aaron Saunders and Meyer Nahon [20] analyzed the effect of forward vehicle velocity on the tunnel thruster performance, and the test model is established according to C-SCOUT FAC. Other spherical underwater robots have used water-jet thrusters instead. Researchers at Harbin Engineering University developed a spherical underwater robot with three water-jet thrusters [21, 22]. However, the propulsive force of the thrusters was considerably reduced because the water input pipeline was curved. Researchers at the Beijing University of Post and Telecommunications developed a spherical

Table 1 SUR-II main parameter

Parameter	Value
Diameter (m)	0.4
Weight in air (kg)	6.5
Max speed (cm/s)	30
Min speed (cm/s)	0
Dive rate (cm/s)	15
DOF	6
Power consumption(W)	10

underwater robot with one tunnel propeller [23]. This robot adjusted its attitude by changing its center of mass through a movable weight-balancing block, which made it possible to adjust the direction of the tunnel propeller and achieve some underwater motion. However, the robot could not perform hybrid motions because it only had one propeller, and the movable weight-balancing block required a long response time.

1.2 Motivation

Considering the advantages of the spherical shape and tunnel thruster, we wanted to develop an underwater robot for local environment monitoring and operations. The design requirements were that the robot must:

- be small in size: less than or equal to 40 cm;
- produce only low levels of noise: reduce the effect on water environment and creature;
- consume low amounts of power: maximum output 10 w;
- have high shock resistance: deliver it from aircraft or ship directly;
- be able remain stationary at a given position and orientation;
- have at least 4-degree-of-freedom (4-DOF) motion: surge, sway, heave, and yaw;
- have a turning radius of 0 mm: in underwater narrow space or water transportation pipe.

The main parameter is shown in Table 1.

Based on these requirements, we designed and developed a second-generation spherical underwater robot (SUR-II) that used three vectored water-jet thrusters for its propulsion system [24–28]. The body coordinate system is shown in Fig. 1. The robot consisted of a sphere 400 mm in diameter with three holes to allow water to flow in and out of the robot. The propulsion system, which consisted of three vectored water-jet thrusters, was different from other traditional propulsion methods.

1.3 Outline

The remainder of this paper is organized as follows. Section 1.2 introduces the mechanical structure of the entire robot, with a focus on the structural features and the propulsion system. The master–slave electrical system is introduced in Section 2, compare with the generation I. A 3-axis MEMS IMU is employed to enhance the performance of SUR-II. Sensor data calibration by Kalman filter is also proposed in this section. This section also presents the software design, along with the communication laws between the slave processor and the master processor. Section 3 describes the underwater experiments used to verify the performance of the spherical underwa-

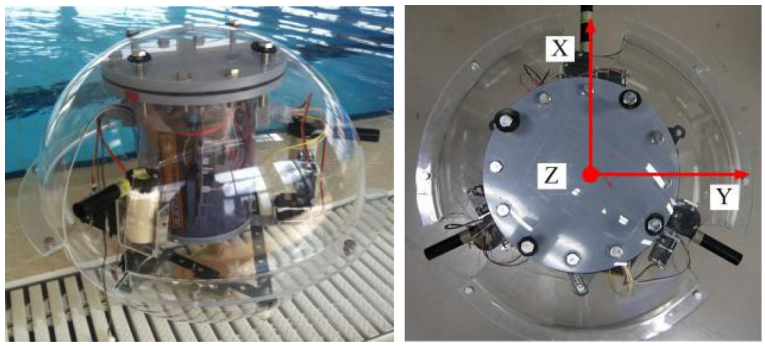

(a) side view (b) top view

Fig. 1 Prototype of the second-generation spherical underwater robot (SUR-II)

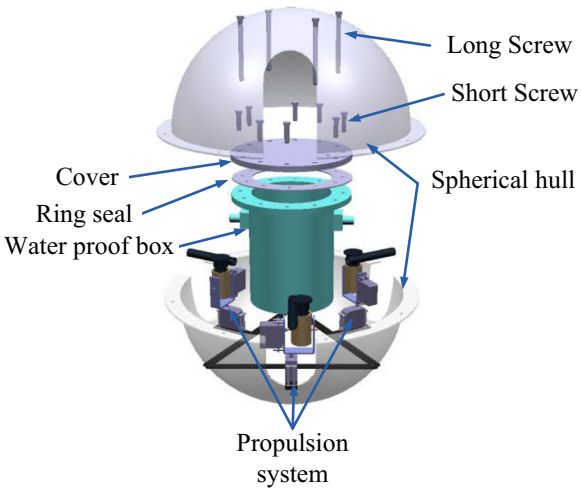

Fig. 2 Conceptual design of the SUR-II

ter robot when we only control the direction of the thrusters, and Section 4 discusses our conclusions and future work.

2 Mechanical Design

2.1 Structure of the SUR-II

The diameter of the SUR-II (D) was 400 mm, and the volume of the cylindrical pressure vessel was D 140 mm × 200 mm. Two hemispheric hulls were used as a protecting shell to keep the robot safe and stable. A detailed illustration of the robot is shown in Fig. 2. The pressure vessel was supported by four 100-mm-long screws. Because the pressure vessel was large and light, the box determined the buoyancy of the robot. Because the position of the pressure vessel could be adjusted by the four long screws, the center of buoyancy was also adjustable. Therefore, we could use this feature to adjust the restoring moment. The cover of the pressure vessel was fixed by eight short screws to prevent water from flowing into the box. A ring seal was also used to enhance the sealing performance. Ensuring a waterproof seal between the pressure vessel and the control cables was a challenge; we employed waterproof silicone to fill the gaps between the cables and the holes required to connect the external thruster units and mount the sensor. The propulsion system was fixed to the lower hemisphere, and the electrical system was protected by the pressure vessel.

2.2 Propulsion System of the SUR-II

The propulsion system is one of the most important parts of an underwater robot because all motion depends on it. The propulsion system was composed of three vectored water-jet thrusters and a triangular support. The triangular support was fixed to the lower spherical hull. Detailed information about the propulsion system is shown in Fig. 3. We installed the propulsion system within the spherical hull, which differs from traditional systems, for three reasons.

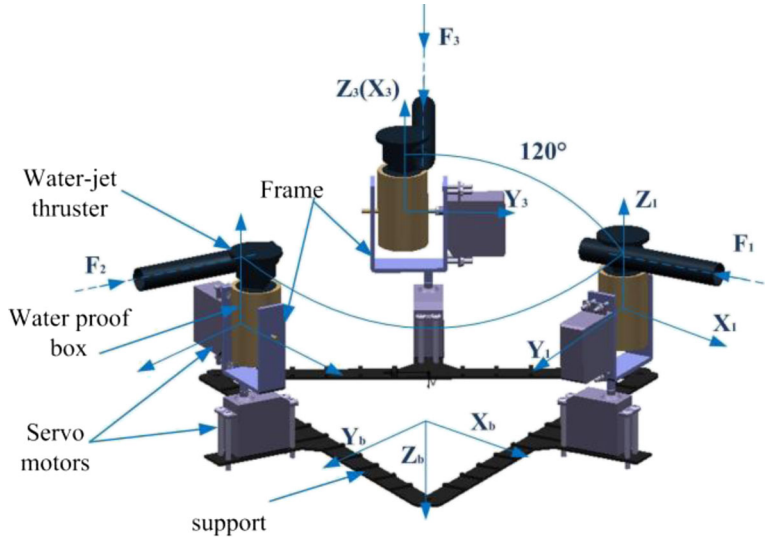

Fig. 3 Structure of the propulsion system

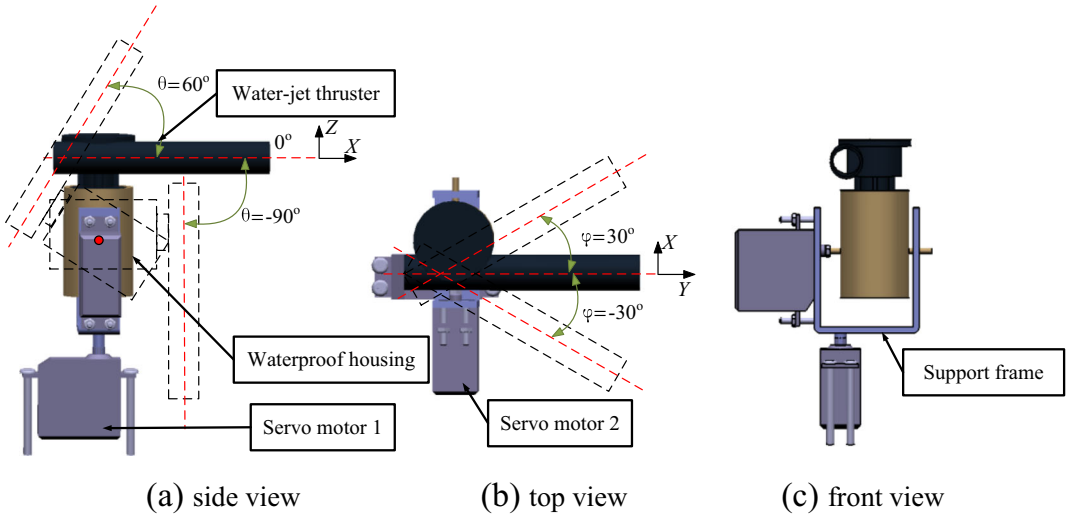

Fig. 4 Vectored water-jet thruster

First, underwater environments are complex, and a variety of creatures live in the water. Having the propulsion system installed within the hull can effectively prevent external impacts. Second, comparing with outside configuration, e.g. ODIN-III [13], with this arrangement, the hull of the robot can be designed to approximate a sphere, reducing the influence of the propulsion system on the hydrodynamic characteristics of the robot. Third, this design makes the robot compact.

The vectored water-jet thrusters provided satisfactory motion control performance. As shown in Fig. 4, each vectored water-jet thruster was composed of five components: the water-jet thruster, one waterproof housing, two servomotors, and one support frame. The water-jet thrusters provided the propulsive force for the SUR-II. The servomotors were employed to change the direction of each thruster. The waterproof housing protected the direct current (DC) motor for each water-jet thruster from the water. Each vectored water-jet thruster provided 2-DOF motion. Figure 4a shows the range of rotation from -90 to $+60°$ in the vertical direction. Vertical motion of the SUR-II was possible due to the rotational DOF in the vertical direction. Figure 4b shows the range of rotation in the horizontal direction, which was 60°. The detail information showed in Table 2. The servomotors not only adjusted the thruster orientation but also generated resistance torque to ensure that the thruster orientation remained correct.

3 Electronic System Design

The SUR-II is our second-generation spherical underwater robot. The first generation was designed and developed by Lin [29–31]. The SUR-II is improved in terms of both its mechanical structure and electronic system. We have previously analyzed the mechanical features and hydrodynamic features of the SUR-II [32]. In this paper, we will compare the two generations of spherical underwater robots in terms of their electronic systems.

The robot can be divided into four subsystems: the mechanical, propulsion, control, and sensor systems. We introduced the mechanical and propulsion systems

Table 2 Main features of the actuators

Motors	Motion range (degree)	Max output	DOF
Servomotor 1 HS5646WP	$\varphi \in \{-30 \sim +30\}$	Torque:12.9N*cm	1
Servomotor 2 HS5646WP	$\theta \in \{-90 \sim +60\}$	Torque:12.9N*cm	1
Water-jet thruster	-	Propulsive force: ±2N	2

in Section 1.2. In this section, we present details of the sensor and control systems. The purpose of this robot is to provide underwater monitoring and operations. However, we do not describe the sensors for these tasks in this paper; rather, we focus on the sensors for motion control and data collection. For motion control, the surge, sway, heave, roll, pitch, and yaw, $\eta = [x, y, z, \theta, \gamma, \psi]^T$, must be calculated for all six DOFs. Although the roll and yaw motions are seldom used, these two parameters should also be obtained and can be used for stability criteria. For example, if the robot has no active roll or pitch motion but the sensor output indicates large values, we can infer that the robot is affected by turbulence or other noise. Of course, if the roll and pitch motions are driven by the propulsion system, the roll and pitch angles cannot be used as stability criteria.

3.1 Sensors

A gyroscope and compass are the most suitable sensors for attitude measurement and stabilization. Many types of inertial measurement units (IMUs) have been developed to satisfy the requirements of different vehicles. In the SUR-II, which was limited by the size of its pressure vessel and by cost, fiberoptic or machined gyroscopes were replaced by an ADIS16365 microelectromechanical system (MEMS) IMU, which is small and inexpensive, as shown in Fig. 5a. The MEMS IMU contained three gyroscopes, three accelerometers, and three temperature sensors. However, the temperature sensor was used not to measure the temperature of the environment but for temperature compensation for the gyroscope and accelerometer. In the original SUR, only one gyroscope was employed to obtain the angle information in the yaw direction, as shown in Fig. 5b.

Depth and altitude sensors are always used in underwater robots. The spherical underwater robot was designed for shallow water, where the water depth was about 10 m. The accuracy of the depth sensor affects the location accuracy of the robot. Therefore, the measurement range of the depth sensor should suitable for this design requirement In the SUR-II, a small high-accuracy depth sensor was selected, as shown in Fig. 5c.

3.2 Sensor Data Calibration

An effective filter must be applied during data preprocessing to reduce the noise from the MEMS IMU sensor. Butterworth and Kalman filters are common methods of data processing. The Butterworth filter works well on fixed-frequency noise, whereas the Kalman filter provides an optimal recursive data processing algorithm. Therefore, we considered each of these two filters, and compared their data-processing performance in tests. The original data collected from the IMU sensor were processed using each of the two filters, and the results were compared. The sensor remained in a static state during the tests, and the Z-axis in Fig. 1b matched the heave direction when we collected the data. Therefore, the sensor output was only affected by the rotation of the Earth and gravity. The rotation of the Earth is constant at 0.04°/s and can be ignored for the short duration of these tests. Gravity is variable at different latitudes and altitudes. The relationship between gravity and latitude can be expressed using D'Alembert's formula [31]:

$$g(L) = g_0(1+0.0052884\sin^2 L - 0.0000059\sin^2 2L), \quad (1)$$

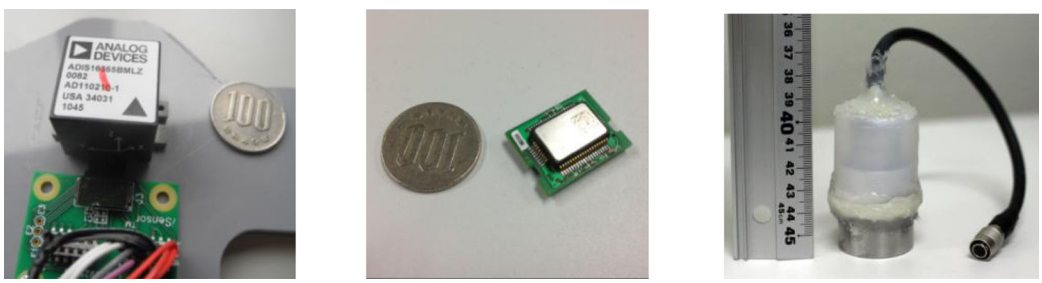

(a) MEMS IMU for the SUR-II (b) MEMS gyroscope for the SUR (c) XP-7001MB depthsensor

Fig. 5 The main sensors

and the relationship between altitude and gravity can be calculated by

$$g(H) = \frac{g_0 R^2}{(H+R)^2}. \quad (2)$$

Here, $g_0 = 9.78049$ is standard gravity, L is the latitude, R is the radius of the Earth, and H is the altitude of the experimental field. Our field test took place in Takamatsu, Japan; the longitude (B) and latitude (L) were $E134°\ 03'\ 48.91''$ and $N34°17'38.50''$ respectively, and the altitude (H) was 22.88 m. As the robot was designed to work in shallow water, the maximum difference in altitude was only about 10 m. Given that the radius of the Earth is 6378 km, from Eq. 2, the

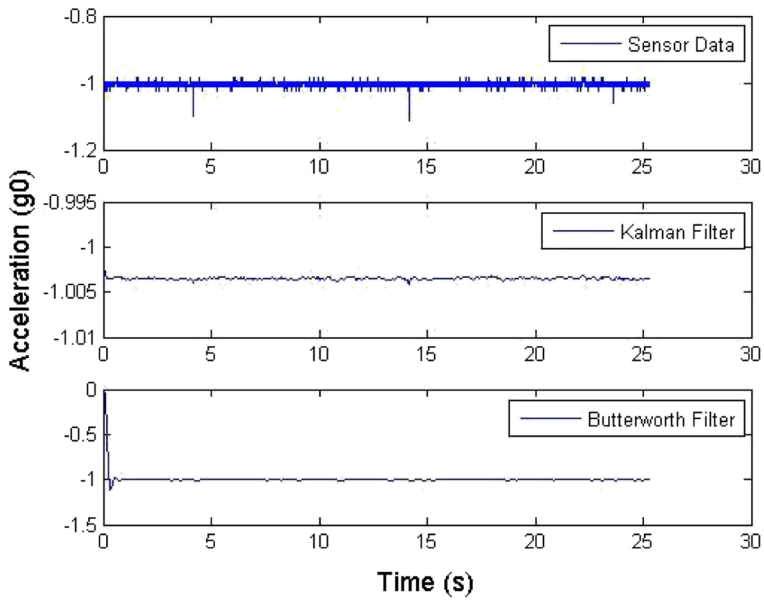

(a) Acceleration along the Z-axis

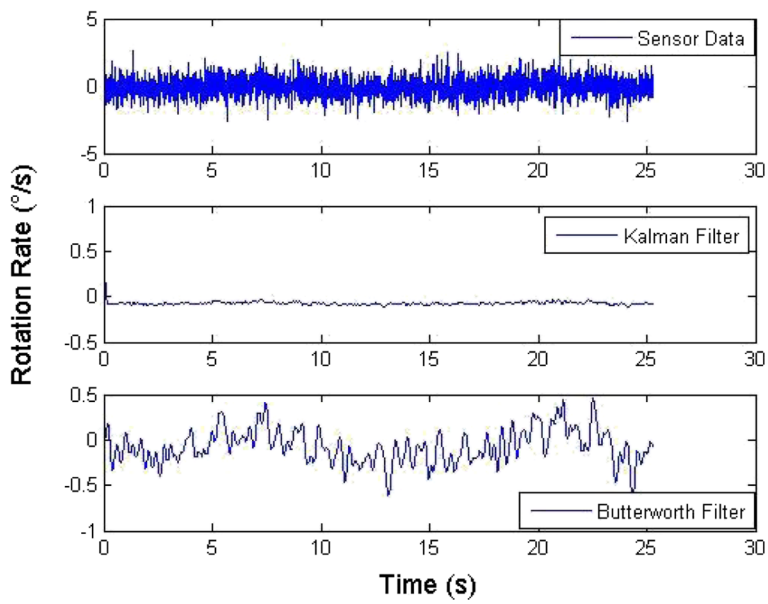

(b) rotation rate in the XY plane

Fig. 6 Comparison of the Kalman and Butterworth filters

altitude had almost no effect on gravity. Therefore, D'Alembert's formula alone could be used to describe gravity. Thus, gravity for the experimental field was $g = 1.0016 g_0$.

Figure 6a shows the acceleration of the Z-axis. Because the sensor was in a static state, the sensor output should have been equal to the acceleration of gravity. However, the sensor data contained some noise. After applying the Kalman filter, we obtained $g = 1.003\ g_0$, which was about 0.1 % greater than the theoretical value. The Butterworth filter also provided good suppression of the high-frequency noise from the accelerometer but required a short adjustment time.

Figure 6b shows the rotation rate of a gyroscope in the XY plane. As the Z-axis coincided with the heave direction, the rotation in the XY plane can be defined as the yaw motion. The output should be 0 because the sensor was in a static state. There was a lot of noise in the raw sensor data. Here, the Kalman filter performed better than the Butterworth filter, and the resulting data were much closer to 0 compared with the results obtained using the Butterworth filter. Additionally, the Kalman filter is a time domain filter, which is easy to implement using the existing hardware. The Butterworth filter is a frequency domain filter. Therefore, we used the more efficient Kalman filter to carry out the data preprocessing for the SUR-II.

We also tested the accuracy of the depth sensor and obtained the error between the theoretical and measured values. The principle of the depth sensor was based on the measured pressure. Therefore, we tested the depth sensor using a series of different pressures to simulate different water depths. The results are shown in Table 3. Because the depth sensor was highly accurate and its error was very small, we compensated for depth sensor error using only a simple linear compensation method. After compensation, the measurement error was about 0.5 cm.

3.3 Control Circuit Design

The structure of the control circuit was designed using a master–slave configuration. Thus, the control circuit was divided into a master side and a slave side. The master side was used for sensor data collection, control algorithm realization, and command transmission. The slave side was used to execute the commands from the master side and to drive the actuators to execute underwater missions.

The control circuit of the original SUR is shown in Fig. 7. The ARM S3C44b0x01L and Atmega2560 processors were employed as the master and slave processors, respectively. The power was supplied by one lithium battery.

The details of the control circuit for the SUR-II are shown in Fig. 8. Unlike the original SUR, a TMS 320f28335 processor was employed as the master processor. This processor is better than the ARM in two respects. First, the dominant frequency can reach 150 MHz, allowing us to reduce the computing time and realize a more complex control algorithm. Second, the TMS 320f28335 processor supports floating-point arithmetic and is more suitable for data fusion and optimization.

The DC motor, which was used to generate the propulsive force, consumes more energy than any

Table 3 Pressure sensor feature

Pressure (Kpa)	Depth in theoretical value (cm)	The actual measured value (cm)	Error (cm)
0.00	0.00	0.4	-0.40
25.00	254.93	255.2	-0.27
50.00	509.86	510.4	-0.54
75.00	764.79	765.3	-0.51
100.00	1019.72	1020.2	-0.48
120.00	1223.66	1224.2	-0.54
100.00	1019.72	1020.2	-0.48
75.00	764.79	765.3	-0.51
50.00	509.86	510.3	-0.44
25.00	254.93	255.3	-0.37
0.00	0.00	0.2	-0.20

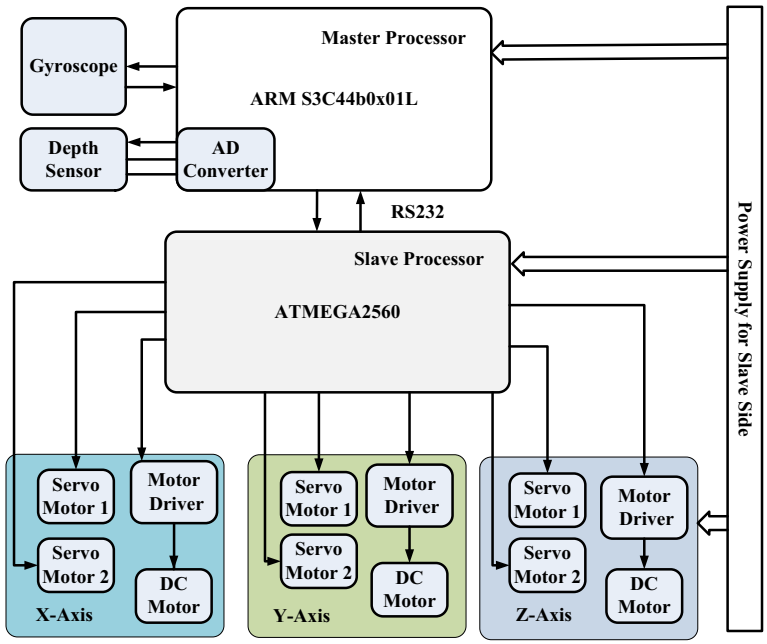

Fig. 7 Block diagram of the original SUR prototype control circuitry

other component in the robot. Because we used three DC motors, a high-storage battery was required. Our configuration method prevented mutual interference.

Figure 9 shows the electrical system used for the SUR-II. Any errors in the installation of the IMU sensor will affect navigation accuracy, so the mounting

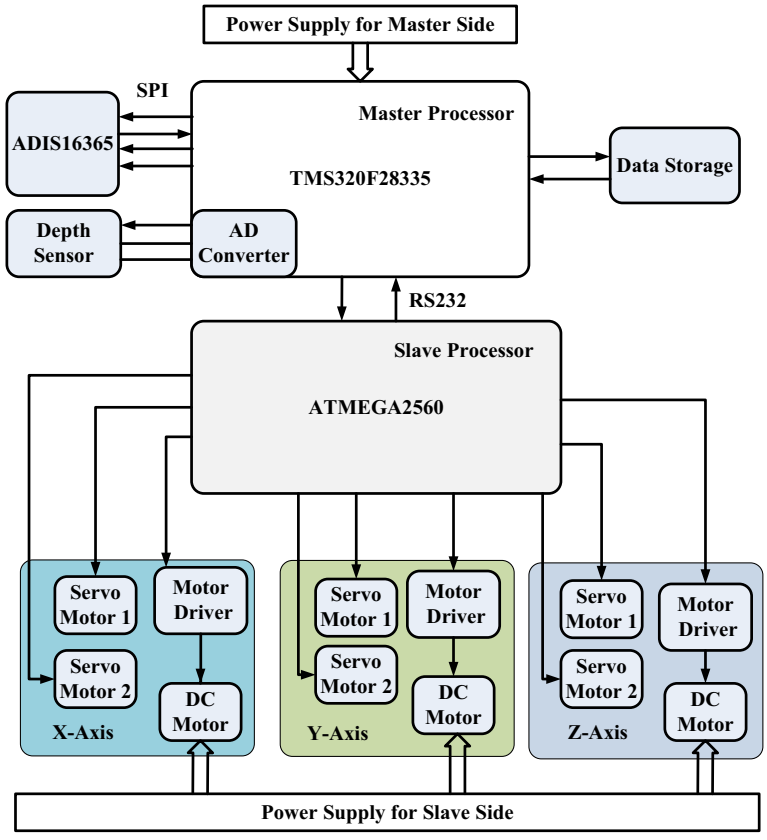

Fig. 8 Block diagram of the SUR-II prototype control circuitry

Fig. 9 Electrical system

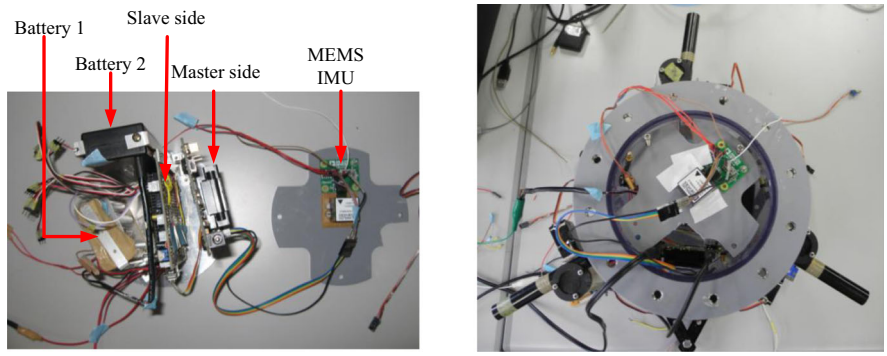

(a) main parts of the electrical system (b) electrical and propulsion systems combined

position of the sensor was fixed at the geometric center of the robot, as shown in Fig. 9b.

Comparison with the previous electrical system, the new electrical system can get 3-axis acceleration, 3-axis angle, 3-axis temperature, and depth information. Based on the new processor and the principle of strap down inertial navigation, the orientation, velocity and position can be obtained. Comparison with the previous electrical system, the computing power is increased about 2.5 times. Two angle parameters are employed to judge the stability of the robot.

3.4 Software Design

The propulsive force could be controlled by the direction of the water-jet thrusters or by the magnitude of the forces exerted by the thrusters. In this paper, we only controlled the direction of the thrusters to test their performance, and we combined the three propulsive forces to implement underwater motion. The thrusters were set to their maximum output.

We used a proportional-derivative (PD) controller to control the direction of the thrusters and enhance their flexibility. Figure 10 shows a simplified flow chart of the control strategy. For a given task, the robot first completed its system initialization, which involved initializing and calibrating the sensors. After initialization, the initial attitude angle, depth, and position were obtained. The robot then compared the current parameters with the target parameters. If the current parameters were not equal to the target parameters, the robot attempted to reduce the differences through motion by calculating a suitable trajectory.

We also designed the communication laws between the master side and the slave side to control the vectored water-jet thrusters. The details are listed in Table 4. In the table, bits 0, 7, and 8 are used to check the parity. Bit 1 determines which type of motor is selected: the DC motor, servomotor 1, or servomotor 2. Bit 2 determines which motors are driven to realize motion. Bits 3, 4, and 5 contain the commands to the motor selected by bit 2.

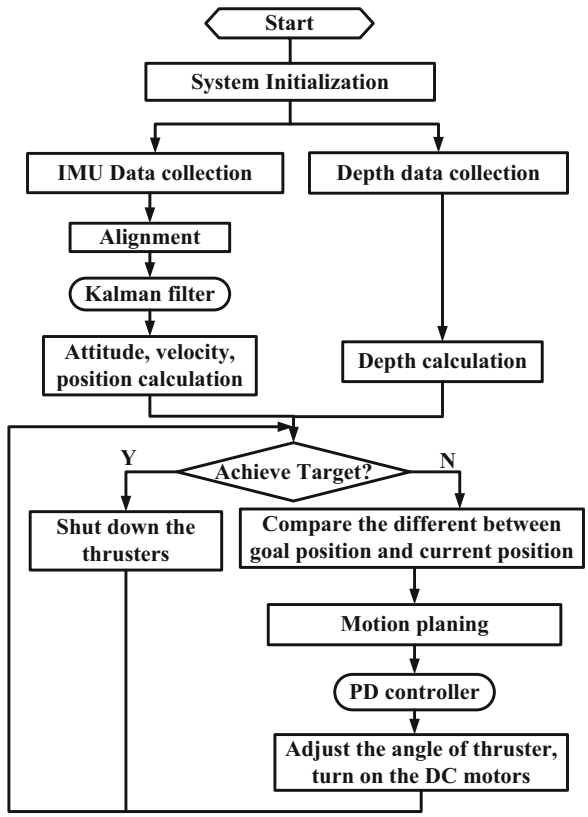

Fig. 10 Simplified flow chart of the software structure

Table 4 Communication laws

Start bit	Motor selected	Motor number	Command
53	XX	XX	XX
0	1	2	3
Command	Command	End bits	
XX	XX	50	ff
4	5	6	7

4 Underwater Experiments

Underwater experiments were carried out to test the performance of the SUR-II. The tests field was in a 25 × 15 × 1.1 m pool and water temperature was 20°. For our robot, we can control the magnitude and direction of the thrusters, but in these experiments, we only control the direction of the thrusters to implement the underwater motion to verify the feasibility of the vectored water-jet thrusters. The thruster configuration is shown in Fig. 11. $\Phi = \left[\phi_1\ \phi_2\ \phi_3\right]^{\mathrm{T}}$, $\Theta = \left[\theta_1\ \theta_2\ \theta_3\right]^{\mathrm{T}}$ are the control variables for the experiments. For the surge motion, F_2 and F_3 generate the propulsive force F_{surge} and torque in yaw direction can be expressed as follows.

$$F_{surge} = F_3 \cos(\frac{\pi}{3} - \phi_3) + F_2 \cos(\frac{\pi}{3} - \phi_2) \tag{3}$$

$$T_{yaw} = F_3 \times R \sin\phi_3 - F_2 \times R \sin\phi_2 \tag{4}$$

Where R is the radius of the robot; F_3 is equal to F_2; the size of the propulsive force F_{surge} is decided by the angle of the thrusters. Therefore, we can control the speed by adjusting φ_2 and φ_3 synchronously. Of course, the φ_2 is always equal to φ_3 to keep balance in yaw direction, T_{yaw} =0. But, if the robot is affected by environment and an undesired yaw motion is generated. The robot will detect the angle error and adjust the φ_2 and φ_3 to generate a torque, T_{yaw}. The torque will drive the robot to reduce the angle error.

4.1 Surge Motion

The drag coefficient of a spherical object is about 0.4 [33], so the water resistance is strong in the surge direction. But in the yaw direction, the water resistance torque is very small because a spherical object is centrosymmetric. It is therefore easy to generate rotational motion of a spherical object. In the SUR-II, the included angle between two thrusters for surge motion was 120°, so it was difficult to realize linear motion in the surge and sway directions without closed-loop control. Thus, the first test was used to test linear motion in still water. The robot was to travel straight without any noise. We used the IMU sensor to detect the altitude angle; if the robot generated an attitude angle in the yaw direction, it was deviating from its original route. The robot used servomotor 1, which controls the direction vector of a water-jet thruster (Fig. 4), to generate a resistance torque and reduce errors in the attitude angle, allowing the robot to move along the intended path. The control variables are the direction of the thruster $\{\varphi_2, \varphi_3\}$ The experimental results are shown in Figs. 12 and 13.

The test lasted 60 s. At the start of the test, the robot generated a rotational motion due to the unequal propulsive forces. The robot then adjusted its

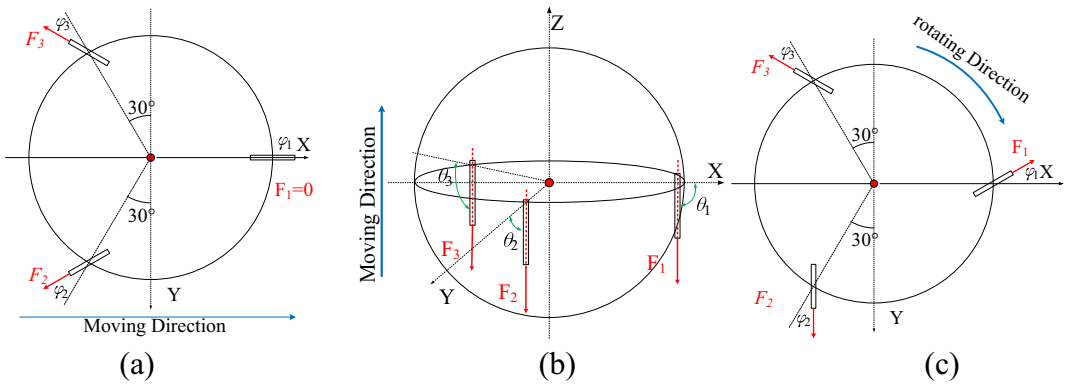

Fig. 11 The thruster configuration in the experiments

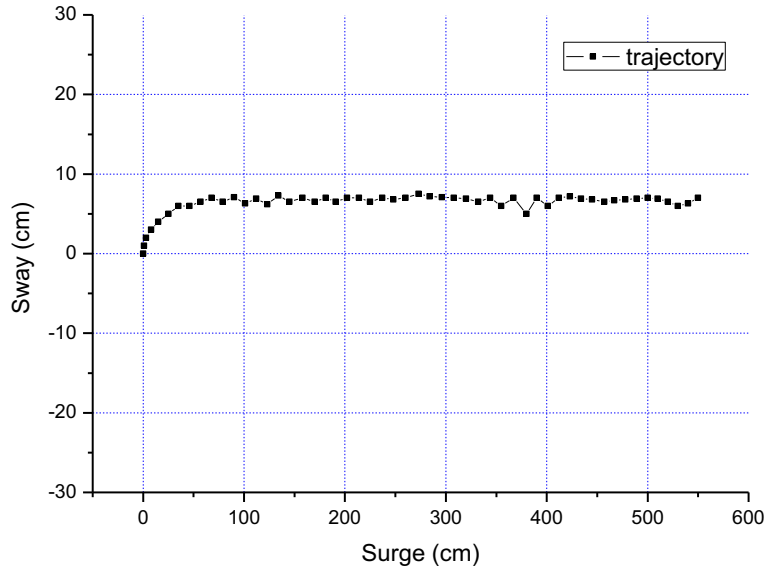

Fig. 12 Trajectory of surge motion

attitude after detecting the angular error. Although the angular error was eliminated immediately, the robot could not turn back to its original trajectory. Thus, this closed-loop control method could not reduce the displacement error, but could prevent the error from growing.

4.2 Yaw Motion

This test was used to test the flexibility and stability of the robot in the yaw direction. Due to the spherical hull, the water resistance was very small in the yaw direction; therefore, it was straightforward to adjust the attitude of the robot. The IMU sensor was also employed to measure the rotational angle. The robot was stable at the start of the test. Then, we freely rotated the robot in the yaw direction. The sensor detected the angle difference, and the three vectored water-jet thrusters turned in the opposite direction to generate resisting torque to maintain the desired attitude. As the angle difference was reduced, the angle of the thrusters turned back to reduce the moment in

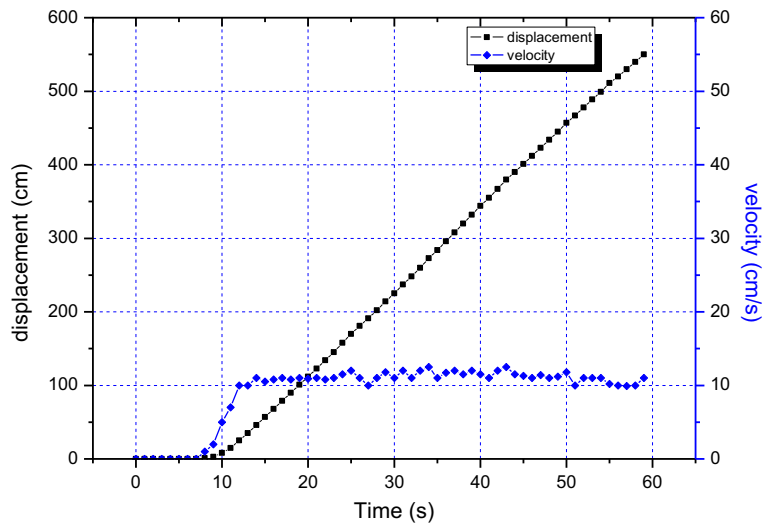

Fig. 13 Velocity and displacement during surge motion

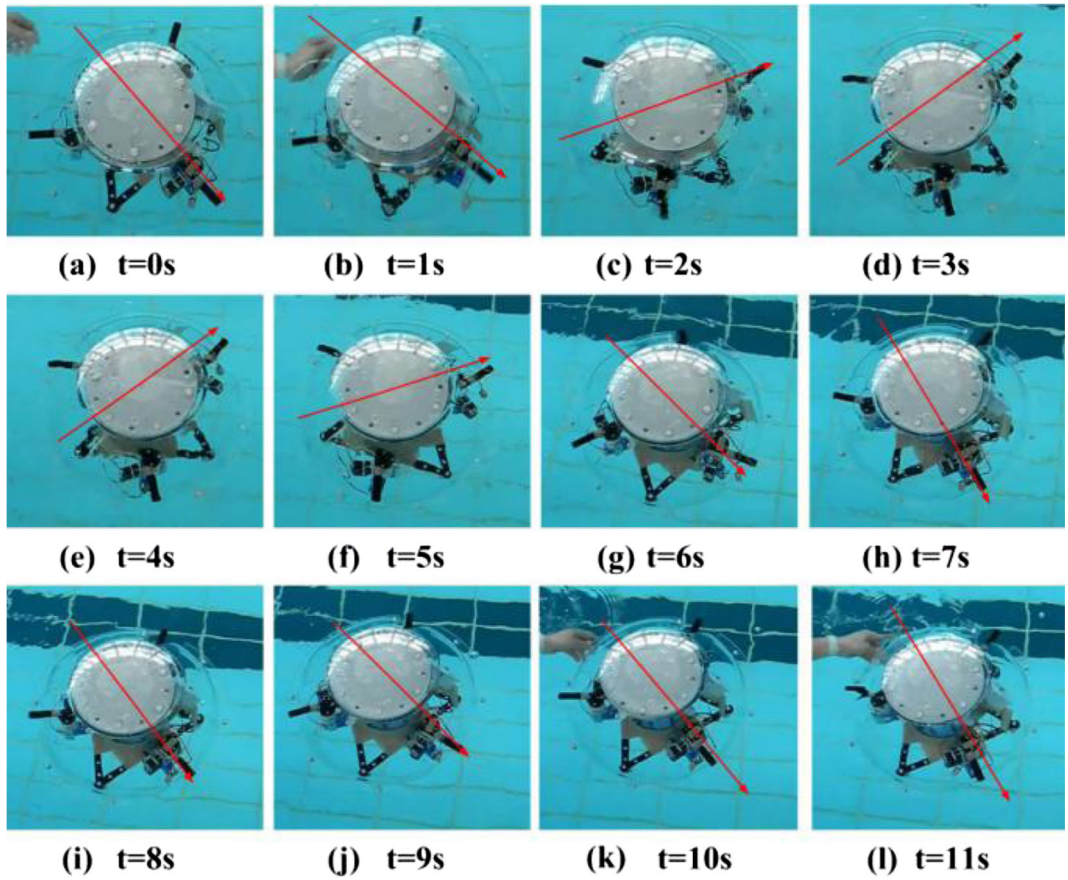

Fig. 14 Yaw motion test

Fig. 15 Experimental results in the yaw direction

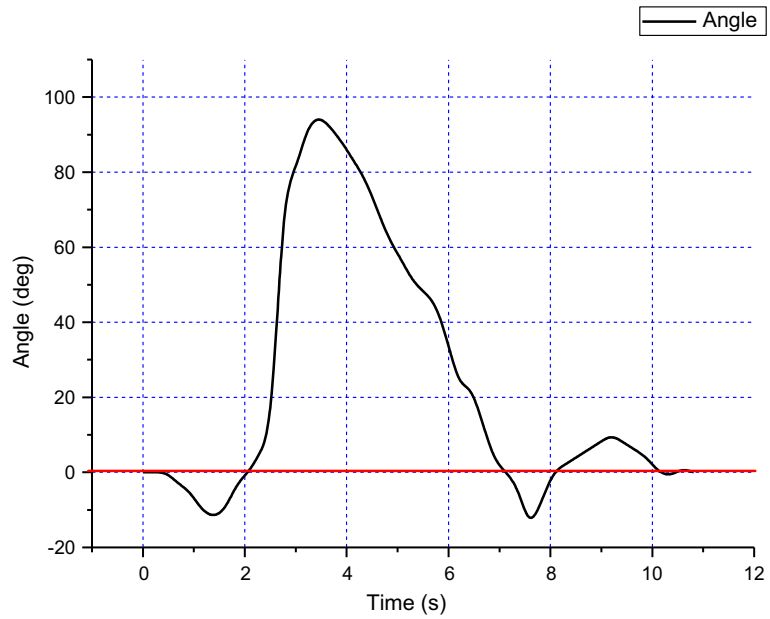

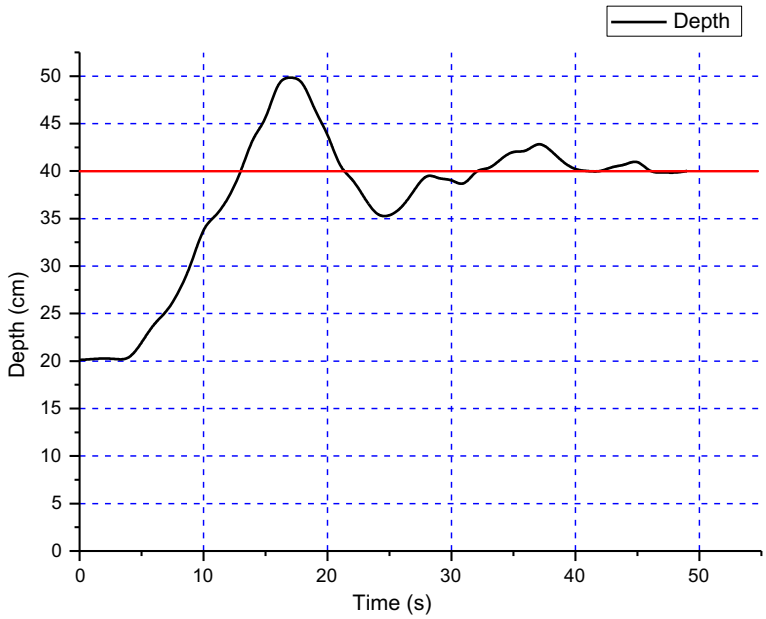

Fig. 16 Experimental results of depth control

the yaw direction. Finally, the robot stopped when it was oriented in the original direction and the torque was reduced to 0. The control variables are the direction of the three thrusters in horizontal position $\{\varphi_2\varphi_3\}$ The results are shown in Figs. 14 and 15. In Fig. 14, the red arrows indicate the surge direction of the robot. The PD controller successfully realized the simple direction control for the vectored water-jet thrusters of the SURII, as shown in Fig. 15. The response time of the robot was only 10 seconds because the water resistance was small.

4.3 Depth Control

A depth control test was used to verify the accuracy and response time of the SUR-II. The robot started at a depth of 20 cm, and was to move to a depth of 40 cm and hold its position at that location. The pressure sensor was installed under the pressure vessel. We corrected for the difference between the location of the depth sensor and the geometric center of the robot in the control algorithm. The robot reached the desired depth after 25 s, based on a 5-cm tolerance

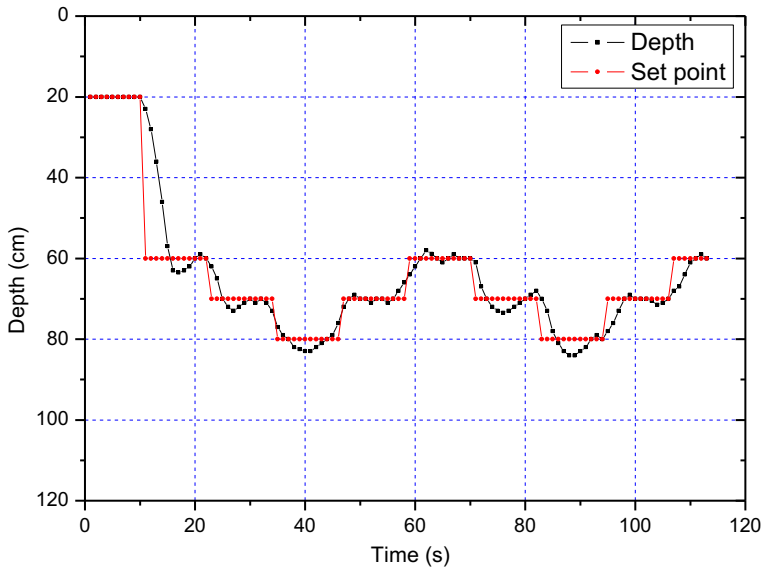

Fig. 17 Experimental results of multiple-depth control

for error, and after 40 s based on a 2-cm tolerance, as shown in Fig. 16.

4.4 Multiple Depths

Since the robot may be required to work at different depths to perform one task, we conducted a test using multiple depths. In this test, we assumed that the robot had three target positions at different depths. The robot started by floating on the surface. Then, the robot was to descend to depths of 60, 70, and 80 cm, stopping at each depth for a few seconds, and then return to depths of 70 and 60 cm. This pattern was then repeated. We only controlled the direction of the vectored water-jet thrusters, not the amount of thrust, to verify the underwater motion performance of the robot. We corrected for the difference between the location of the depth sensor and the geometric center of the robot.

The results are shown in Fig. 17. The red line gives the set point for the motion control, and the black line gives the actual depth of the robot. The system initialization and sensor calibration were completed at the start of the test. About 10 s later, the robot was driven to its first depth. Because the robot had a large amount of inertia in the water, the maximum overshoot of the experiment was about 5 cm. The change in the direction of the propulsive force was nonlinear due to the control variables, resulting in a robot trajectory that corresponded to simple harmonic motion. At least 10 s were required to reach an acceptable stable state at each depth.

5 Conclusion and Future Work

We developed a spherical underwater robot, the SUR-II, driven by only three vectored water-jet thrusters to implement underwater motion. We designed and developed the robot by taking advantage of the good water and shock resistance properties of a sphere. Due to the low power and low noise design requirements, we used three vectored water-jet thrusters driven by two servomotors. The three thrusters were uniformly arranged around the equator of the robot so that the robot could realize 4-DOF motion by combining the three thrusters. We improved the electrical system by changing the MEMS sensor, master processor, and electrical structure of the original SUR. The electrical system could obtain three attitude angles from a MEMS IMU, and the roll and pitch angle could be used to judge the stability of the robot. We employed a Kalman filter for data preprocessing to reduce the noise generated by the MEMS sensor. A series of underwater experiments were carried out to test the performance of the spherical underwater robot. The experimental results demonstrated that the robot could realize surge, yaw, and heave motion within a tolerable error only by control the direction of the thrusters.

In the future, we plan to use a more efficient adaptive proportional–integral–derivative (PID) controller to control the direction of the thrusters and improve the depth control. We will also consider adjusting the magnitude of the propulsive forces as well as their directions to enhance the control accuracy and stability of the robot.

Acknowledgments This work was partly supported by National Natural Science Foundation of China (61375094), and Key Research Program of the Natural Science Foundation of Tianjin (13JCZDJC26200).

The English in this document has been checked by at least two professional editors, both native speakers of English. For a certificate, please see: http://www.textcheck.com/certificate/XIKugh

References

1. Wang, S.X., Sun, X.J., Wang, Y.H.: Dynamic modeling and motion simulation for a winged hybrid-driven underwater glider. China Ocean Eng. **25**(1), 97–112 (2011)
2. McPhail, S.: Autosub6000: A Deep Diving Long Range AUV. J. Bionic Eng. **6**, 55–62 (2009)
3. Steenson, L.V., Phillips, A.B., Furlong, M., Rogers, E., Turnock, S.: The performance of vertical tunnel thrusters on an autonomous underwater vehicle operating near the free surface in waves. Second International Symposium on Marine Propulsors (2011)
4. Avila, J.P., Donha, D.C., Adamowski, J.C.: Experimental model identification of open-frame underwater vehicles. Ocean Eng. **60**, 81–94 (2013)
5. Pan, Q., Guo, S., Okada, T.: A novel hybrid wireless microrobot. Int. J. Mechatron. Autom. **1**(1), 60–69 (2011)
6. Philips, A.B., Steenson, L.V., Rogers, E., Turnock, S.R., Harris, C.A., Furlong, M.: Delphin2: an over actuated autonomous underwater vehicle for manoeuvring research. Trans. Royal Inst. Naval Architects, Part A - Int. J. Marit. Eng. **155**(A4), 171–180 (2009)
7. Curtis, T.L., Perrault, D., Williams, C., Bose, N.: C-SCOUT: a general-purpose AUV for systems research. in Underwater Technology, 2000. UT 00. Proceedings of the 2000 International Symposium on, pp. 73–77 (2000)
8. http://www.auvac.org/community-information/community-news/view/2462

9. Sanz, P.J., Prats, M., Ridao, P., Ribas, D., Oliver, G., Orti, A.: Recent progress in the RAUVI Project. A Reconfigurable Autonomous Underwater Vehicle for Intervention, 52th International Symposium ELMAR-2010, vol. 471–474, Zadar, Croatia (2010)
10. Packard, G.E., Stokey, R., Christenson, R., Jaffre, F., Purcell, M., Littlefield, R.: Hull inspection and confined area search capabilities of REMUS autonomous underwater vehicle. in OCEANS (2010)
11. Allen, B., Stokey, R., Austin, T., Forrester, N., Goldsborough, R., Purcell, M., Von Alt, C., vol. 2, pp. 994–1000 (1997)
12. Choi, H.T., Hanai, A., Choi, S.K., Yuh, J.: Development of an underwater robot, ODIN-III In: Proceedings of the 2003 IEEE International Conference on Intelligent Robots and Systems, pp. 836–841 (2003)
13. Choi, S.K., Yuh, J.: Application of non-regressor-based adaptive control to underwater robots: experiment. Comput. Electr. Eng. **26**, 187–194 (2000)
14. Watson, S.A., Crutchley, D., Green, P.N.: The mechatronic design of a micro-autonomous underwater vehicle (μAUV). Int. J. Mechatron. Autom. **2**(3), 157–168 (2012)
15. Watson, S.A., Crutchley, D., Green, P.N.: The Design and Technical Challenges of a Micro-Autonomous Underwater Vehicle (μAUV). In: Proceedings of the 2011 IEEE International Conference on Mechatronics and Automation, pp. 567–572 (2011)
16. Watson, S.A., Green, P.N.: Propulsion systems for micro-Autonomous Underwater Vehicles (μAUVs) In: Proceedings of the 2010 IEEE International Conference on Robotics Automation and Mechatronics, pp. 435–440 (2010)
17. Watson, S.A., Crutchley, D., Green, P.N.: A De-Coupled Vertical Controller for Micro-Autonomous Underwater Vehicles (μAUVs) In: Proceedings of the 2011 IEEE International Conference on Mechatronics and Automation, pp. 561–566 (2011)
18. Steenson, L.V., Phillips, A.B., Furlong, M.E., Rogers, E., Turnock, S.R.: The performance of vertical tunnel thrusters on an autonomous underwater vehicle operating near the free surface in waves. In procedue of Second International Symposium on Marine Propulsors. Hamburg University of Technology, Hamburg, DE (2011)
19. Palmer, A., Hearn, G.E., Stevenson, P.: Experimental testing of an autonomous underwater vehicle with tunnel thrusters. In: SMP'09 - First International Symposium on Marine Propulsors, vol. 6, Trondheim, Norway (2009)
20. Saunders, A., Nahon, M.: The effect of forward vehicle velocity on through-body AUV tunnel thruster performance. In: OCEANS '02 MTS/IEEE (2002)
21. Guo, S., Du, J., Ye, X., Yan, R., Gao, H.: The computational design of a water jet propulsion spherical underwater vehicle In: Proceedings of the 2011 IEEE International Conference on Mechatronics and Automation, pp. 2375–2379 (2011)
22. Guo, S., Du, J., Ye, X., Gao, H., Gu, Y.: Realtime adjusting control algorithm for the spherical underwater robot. Inf.-An Int. Interdisc. J. **13**(6), 2021–2029 (2010)
23. Lan, X., Sun, H., Jia, Q.: Principle and dynamic analysis of a new-type spherical underwater vehicle. J. Beijing Univ. Posts Telecommun. **33**(3), 20-23 (2010). Chinese
24. Yue, C., Guo, S., Shi, L., Du, J.: Characteristics evaluation of the vertical motion of a spherical underwater robot In: Proceedings of 2012 IEEE International Conference on Robotics and Biomimetics, pp. 759–764 (2012)
25. Yue, C., Guo, S., Lin, X., Du, J.: Analysis and Improvement of the Water-jet Propulsion System of a Spherical Underwater Robot. In: Proceedings of 2012 IEEE International Conference on Mechatronics and Automation, pp. 2208–2213 (2012)
26. Yue, C., Guo, S., Li, M.: Electrical System Design of a Spherical Underwater Robot (SUR-II) Proceeding of 2013 IEEE International Conference on Information and Automation, pp. 1212–1217 (2013)
27. Yue, C., Guo, S., Li, M.: ANSYS FLUENT-based Modeling and Hydrodynamic Analysis for a Spherical Underwater Robot In: Proceedings of 2013 IEEE International Conference on Mechatronics and Automation, pp. 1577–1581 (2013)
28. Yue, C., Guo, S., Li, M.: Yaxin Li: Passive and Active Attitude Stabilization Method for the Spherical Underwater Robot (SUR-II) In: Proceedings of 2013 IEEE International Conference on Robotics and Biomimetics, pp. 1019–1023 (2013)
29. Guo, S., Lin, X., Tanaka, K., Hata, S.: Development and control of a vectored water-jet-based spherical underwater vehicle In: Proceedings of the 201 IEEE International Conference on Information and Automation, pp. 1341–1346 (2010)
30. Lin, X., Guo, S., Tanaka, K., Hata, S.: Underwater experiments of a water-jet-based spherical underwater robot In: Proceedings of the 2011 IEEE International Conference on Mechatronics and Automation, pp. 738–742 (2011)
31. Lin, X., Guo, S., Yue, C., Du, J.: 3D modelling of a vectored water jet-based multi-propeller propulsion system for a spherical underwater robot. Int. J. Adv. Robot. Syst. **10** (2013). doi:10.5772/51537
32. Yue, C., Guo, S., Shi, L.: Hydrodynamic Analysis of a Spherical Underwater Robot: SUR-II. Int. J. Adv. Robot. Syst. **10** (2013). doi:10.5772/56524
33. Houghton, E.L., Carpenter, P.W.: Aerodynamics for Engineering Students Fifth Edition, pp. 8–15. Publishedby Butterworth-Heinemann (2003)